Developmental Cognitive Neuroscience 54 (2022) 101092

Contents lists available at ScienceDirect

Developmental Cognitive Neuroscience

journal homepage: www.elsevier.com/locate/dcn

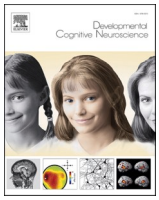

Cortical Source Analysis of Event-Related Potentials: A Developmental Approach

Stefania Conte *, John E. Richards

University of South Carolina, USA

ARTICLE INFO

Keywords:
Source analysis
EEG
Realistic head model
Infancy

ABSTRACT

Cortical source analysis of electroencephalographic (EEG) signals has become an important tool in the analysis of brain activity. The aim of source analysis is to reconstruct the cortical generators (sources) of the EEG signal recorded on the scalp. The quality of the source reconstruction relies on the accuracy of the forward problem, and consequently the inverse problem. An accurate forward solution is obtained when an appropriate imaging modality (i.e., structural magnetic resonance imaging – MRI) is used to describe the head geometry, precise electrode locations are identified with 3D maps of the sensor positions on the scalp, and realistic conductivity values are determined for each tissue type of the head model. Together these parameters contribute to the definition of realistic head models. Here, we describe the steps necessary to reconstruct the cortical generators of the EEG signal recorded on the scalp. We provide an example of source reconstruction of event-related potentials (ERPs) during a face-processing task performed by a 6-month-old infant. We discuss the adjustments necessary to perform source analysis with measures different from the ERPs. The proposed pipeline can be applied to the investigation of different cognitive tasks in both younger and older participants.

1. Introduction

Cortical source analysis of the electroencephalographic (EEG) signal has become an important neuroimaging tool for the localization of functional brain responses across the lifespan. The development of pediatric neuroimaging has been limited by practical and procedural challenges posed by participants in experimental settings. The most widely used technique to localize functional brain responses during cognitive tasks, functional magnetic resonance imaging (fMRI), has been recently adopted in studies with pediatric populations. However, it faces several limitations with very young participants, as fMRI is most successful when infants are asleep or sedated (Raschle et al., 2012). Studies implementing fMRI acquisitions to investigate the neural responses during cognitive tasks were recently applied to awake infants and toddlers performing visual (Ellis et al., 2021a, 2021b, 2021c), attentional (Ellis et al., 2021a, 2021b, 2021c), and statistical learning tasks (Ellis et al., 2021a, 2021b, 2021c). These promising first applications of fMRI protocols are still affected by a high attrition rate and small sample sizes. On the other hand, increased scanning success and fewer procedural difficulties are reported for late toddlers and older participants (Hendrix and Thomason, 2021, Preprint).

EEG is one of the foremost neuroimaging methods in infant research thanks to advances in recording procedures and signal analysis (Vanhatalo and Fransson, 2016). Its high temporal resolution allows EEG to capture the dynamics of neural responses with advantageous applicability to young populations. Moreover, the high temporal resolution of EEG can capture events in the order of milliseconds, without the constraint of the slower hemodynamic response (~seconds) on which the fMRI relies. The poor spatial resolution that characterizes EEG could be overcome by applying source analysis computations to identify the neural generator(s) of the activity recorded on the scalp. Cortical source analysis uses the scalp recording on the outside of the head and computationally infers the sources that generate the signal in the cortex. Accurate modeling of the electrode locations, head geometry, and conductivity properties of the different tissues traveled by the EEG potential determines the accuracy of the source localization. Thus, the combination of functional activity provided by EEG signals (e.g., changes in amplitude and latency), structural anatomy obtained through structural MRI acquisitions, and advanced methods of data processing and analysis define the source analysis approach to the investigation of brain development.

Source analysis procedures could be based on equivalent current

* Corresponding author.
E-mail address: contes@mailbox.sc.edu (S. Conte).

https://doi.org/10.1016/j.dcn.2022.101092
Received 28 May 2021; Received in revised form 16 February 2022; Accepted 22 February 2022
Available online 25 February 2022

dipoles methods or distributed source methods. The equivalent current dipole approach is based on the assumption that the EEG potential can be mimicked as a single or multiple discrete dipoles, the location of which is defined a priori. Such an approach has been implemented to the investigation of cognitive processes, including the developmental changes of late auditory evoked potentials in children and adults. Specifically, both amplitude and latency of peak of dipole activity in response to pure tones showed significant reductions until the age of 16 years. In adults, a new component is generated and reflected in the variability of tangential and radial orientations of the dipoles in the temporal lobe (Albrecht et al., 2000).

Dipole source models have been applied in another study to the investigation of auditory change detection mechanisms in 6-month-old infants. The negative and positive peaks elicited during the discrimination of sounds showed to be localized in the supratemporal and frontal areas (Hämäläinen et al., 2011). In a similar study, the time course of brain activity was evaluated in 6-month-old infants processing speech information (i.e., consonant-vowel syllables). Results showed that infants' responses were localized in similar areas to that reported in adults, but with different timing of activation. The earlier activation of the anterior cingulate cortex compared with the activity in the temporal areas may rely on the difference in the maturation of limbic and cortical areas, with important consequences on the distribution of functional responses to speech sounds (Ortiz-Mantilla et al., 2012). A similar source analysis approach was implemented in the investigation of differences between infants with and without a family history of language and learning impairment (LLI). Different lateralization of the source of auditory signals characterized the brain activity of infants at risk for LLI, in the form of reduced left lateralization and increased right lateralization of the auditory cortex (Cantiani et al., 2019).

The multiple discrete dipole approach was also applied to the source of infants' neural responses in the visual domain to looming danger stimuli. Results showed a pattern of development in the second half of the first year of life (Van Der Weel and Van Der Meer, 2009). The response of the visual cortex differentiates three looming speeds in 10- to 11-month-old infants but not in 5- to 7-month-old infants. Interestingly, an intermediate level of development characterized the neural response of infants at 8–9 months, suggesting a potential relationship between the perceptual abilities for sensing looming danger and infants' improvements in locomotion (Van Der Weel and Van Der Meer, 2009).

Distributed source modeling approach estimates the spatial distribution of neural current over a defined source space, which is usually constrained to the cortical surfaces. This analysis computes the current density across distributed brain areas that together generate the pattern of scalp activity. Several studies implemented the distributed source approach to the EEG recordings with pediatric populations and aimed to investigate a wide range of cognitive tasks (Buzzell et al., 2017; Ladouceur et al., 2006). For instance, distributed source analysis methods were applied to the investigation of covert orienting, familiarization, and visual attention in infants. Pre-saccadic responses of the P1 ERP that were generated in the superior frontal gyrus were sensitive to the validity effect (i.e., larger for cued than un-cued locations), and showed an increase in magnitude between 3 and 5 months of age (Richards, 2005). Neural correlates of attention and recognition memory in infants, represented by the Nc response to familiar and unfamiliar visual stimuli, were localized in the prefrontal and anterior cingulate cortices and modulated by stimulus familiarity (Reynolds and Richards, 2005).

The examination of developmental changes in face-processing in infancy also benefited from the investigation of the neural generators via distributed source analysis methods. The different ERP components involved in the processing of faces (i.e., P1, N290, P400, and Nc) showed specific brain localizations and increased activity in the first year of life. In particular, the N290 component showed similar functional responses and localization to the N170 activity reported in adult studies, suggesting being the most likely neural marker of face processing in infancy (Conte et al., 2020; Guy et al., 2016). Both the N290 and P400/Nc components showed to be involved in the processing of specific emotional faces and localized in the fusiform gyrus and posterior cingulate cortex, respectively (Xie et al., 2019).

Source analysis may be used as a method to assess EEG functional connectivity. Functional connectivity with EEG is typically done on the scalp-electrode level and shows the correlation observed between different electrodes using phase-coupling. Functional connectivity with EEG may be done at the source level. This reveals connectivity between cortical sources rather than scalp locations. Source analysis applied to infant EEG functional connectivity localized the attenuation of the alpha band during periods of attention in regions of the default mode network (Xie et al., 2018). In a similar manner, the distribution of cortical sources in 3-month-old infants detecting changes in object identity and number revealed a similar cortical distribution to the one observed in children and adults. Changes in object identity were localized in areas of the ventral temporal cortex, while changes in number were processed in prefrontal networks (Izard et al., 2008).

Overall, these results show how source analysis may be used in the localization of EEG brain activity recorded on the scalp during a wide range of cognitive tasks and provide further knowledge on the functional organization of the brain. One caution to the use of source analysis with pediatric populations is the need for realistic head models that reflect an accurate representation of the individual's head. The gold standard in this regard is to use structural MRIs from individual participants to construct the fundamental properties of the source analysis. This approach would account for individual differences in the head geometry, which can affect pediatric samples to a larger degree than adults because of the different growth rates to which head and brain changes occur at young ages. For instance, the relationship between brain and skull widely varies between adults and infants. The cranial bones are separated by fontanels and sutures for several months after full-term birth. This characteristic of the human skull assists the growth of the brain and has an impact on the conductivity properties of the compartment (Azizollahi et al., 2020; Flemming et al., 2005; Gargiulo et al., 2015; Lew et al., 2013). The increase in the corticospinal fluid (CSF) in infancy and toddlerhood contributes to the changes in the brain-scalp distance, with important implications on the source signal magnitude (Azizollahi et al., 2016; Beauchamp et al., 2011).

Moreover, the inverse solution can become more precise if individual, realistic head models are used (Vanrumste et al., 2002), especially in those regions that are not well described with spheric models (e.g., temporal lobes), and for studies including clinical samples with structural brain alterations (e.g., lesions, tumors). Additional precautions should be taken by developmental researchers on procedures for electrode locations. EEG net placement can rather vary between young participants, thus the use of standard electrode montage should be avoided.

We provide in the current paper an overview of the processing steps to reconstruct the cortical generators of high-density EEG, discussing some alternative solutions for developmental researchers. We performed an example of distributed source analysis with data from one 6-month-old participant and a representative sample of 12-month-old infants. The proposed source analysis pipeline will be applied to the amplitude values of the P400 ERP component in response to upright and inverted faces and houses. We will discuss alternative approaches to perform source analysis when individual structural MRIs or digital electrode locations are not available. Lastly, we will briefly discuss the adjustment required to conduct source analysis of non-ERP measures (e.g., frequency bands, connectivity) of functional activity. The suggested procedure can be implemented in the investigation of the neural generator of cognitive and perceptual processes in infants and children. Average template-based head models and MATLAB programs are made freely available to use for source analysis in pediatric participants.

2. Source analysis pipeline overview

The EEG potential changes recorded on the scalp are caused by post-synaptic electrical potentials occurring during cortical activity. The potential changes on the scalp are summed electrical activity from a wide variety of sources so that there is not a veridical relation between electrode location on the scalp and the underlying cortical sources. Cortical source analysis methods have been developed as quantitative tools to identify the generator(s) of the cortical activity.

There are several steps to compute the underlying cortical sources from the external scalp recording. These include the so-called forward model that describes how current travels from cortical areas (i.e., source model) through the conductive tissues in the head (i.e., head model) to the electrodes (i.e., electrode placement). The forward model computation results in the lead-field matrix, which describes the relationship between the electrode locations on the scalp (*leads*) and the conductive electrical fields in the head (*fields*)Accurate computation of the forward model requires realistic modeling of the media inside the head. This is best accomplished with a structural MRI of the participant for whom the source reconstruction is being done (Dale et al., 1999). Boundary element (BE; Crouzeix et al., 1999) and finite element methods (FE; Vorwerk et al., 2012) can be utilized to create realistic head models.

Once the forward model constituents are computed, an inverse spatial filter can be constructed to solve the inverse problem. The inverse model multiplies the scalp-recorded EEG/ERP by the inverse spatial filter to generate the pattern of cortical sources inside the head. This step generates many voxels from a minimal set of electrodes. The procedure is defined as the inverse problem and its solution is undetermined. This issue is resolved by selecting parameters to restrict the inverse space computation to theoretical distributions. There are a number of suggested inverse method procedures (e.g., minimum norm estimation, MNE; LORETA; sLORETA; eLORETA; for a review, see Grech et al., 2008).

We use a distributed source analysis method that does not require an assumption on the number of dipoles; the source space is created by using a realistic head model, derived from MRI (Dale et al., 1999); the eLORETA method is used as the inverse constraint. A schematic illustration of the matrices for the forward and inverse computations is shown in Fig. 1.

A visual representation of the source analysis pipeline is reported in Fig. 2 and can be summarized in the following steps:

1. EEG and MRI preprocessing. Accurate MRI selection could be implemented as an alternative to the individual volume if not available.
2. Creation of the 3D coordinates of electrode location and co-registration to the MRI head volume.
3. MRI head volume segmentation using the FE or BE methods as the numerical technique.
4. Calculation of the lead field matrix with the source space limited to the gray matter.
5. Application of the exact low-resolution brain electromagnetic tomography (eLORETA) algorithm to solve the inverse problem.
6. Source estimation and voxel-wise power calculation.
7. Application of the ROI spatial filter to the source values for statistical analyses.

FEM = finite element method; BEM = boundary element method; CDR = current density reconstruction; SVD = singular value decomposition; (o) = optional output.

2.1. EEG and MRI preprocessing

It is critical to obtain data from raw EEG with minimum artifacts for each participant for accurate source reconstruction. Both segmented EEG recordings and averaged ERP datasets can be utilized as input for the source analysis procedure. It is beyond the scope of the current work to discuss the EEG preprocessing procedures in developmental research. Additional details can be found elsewhere (Debnath et al., 2020; Gabard-Durnam et al., 2018). Reliable neural generators can be reconstructed using EEG signals in which the noise from non-brain sources (e.g., eye artifacts) is minimized. Thus, data preparation for source analysis

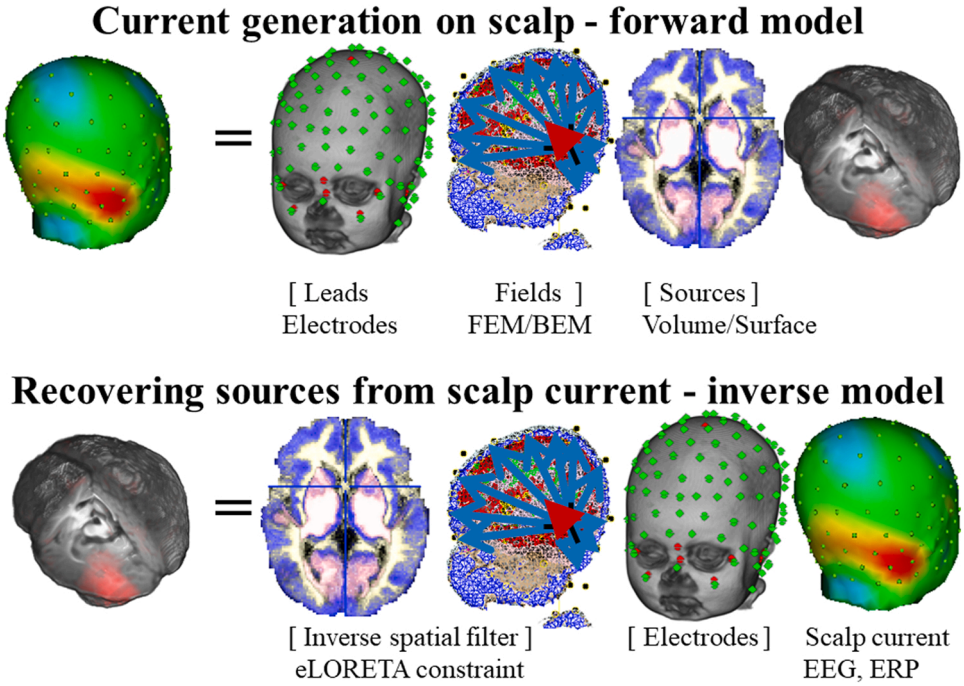

Fig. 1. Schematic illustration of the forward (top) and inverse (bottom) models. From left to right on the top row the elements correspond to the EEG/ERP scalp recording, the electrode locations, the MRI-derived geometry and conductivity of the participant's head, the source space, and the source generators expressed as a current density map.

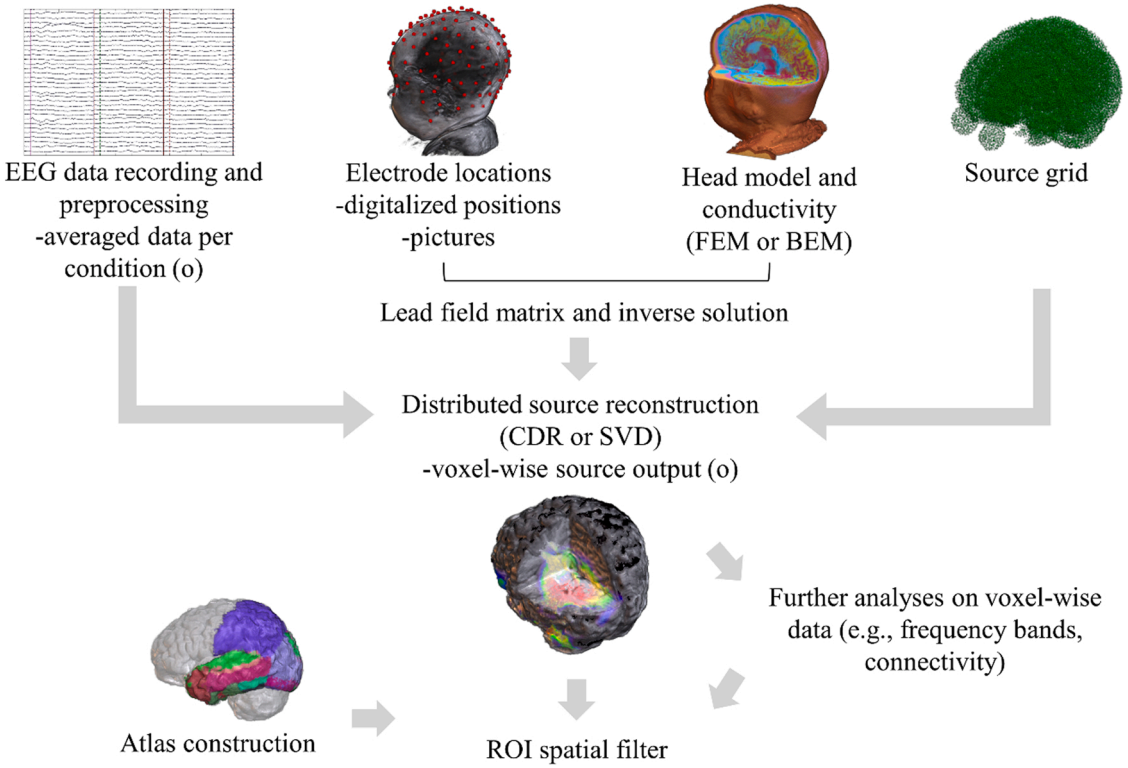

Fig. 2. Schematic representation of the suggested source analysis procedure.

should follow the same principles used to obtain reliable signals for EEG analyses. Moreover, a high-density EEG system would allow the exploration of a wider range of source generators and take into account individual differences in the scalp distributions. We provided evidence in previous works that high-density EEG recordings provide a representation of the electrical scalp potential that a montage with fewer channels would not capture (Gao et al., 2019; Reynolds and Richards, 2009). Similarly, Song and colleagues reported that source solution accuracy increased when electrodes were placed to cover the whole head (i.e., including lower areas of the head) vs. electrode montages restricted to the superior head surface (Song et al., 2015). Thus, the use of a high-density (e.g., 64 channels or higher) and distributed montage is recommended for the implementation of source localization techniques (Seeck et al., 2017; Sohrabpour et al., 2015; Song et al., 2015).

An important step to accurately localize the neural generator(s) of the EEG distribution on the scalp consists in the construction of a realistic head model. Adult anatomy and parameters cannot be directly applied to participants in pediatric studies. The use of individual MRI scans overcomes the localization errors resulting from the use of adult head models for source analysis of pediatric EEG data. Individual MRIs guarantee a description of the head geometry and anatomy tailored to each participant.

The gold standard for source analysis head models is the MRI of the individual participant. However, structural MRI acquisitions can be challenging especially in very young participants, thus limiting the possibility of obtaining good quality images. Two alternative approaches to obtain realistic head models can be implemented when individual MRIs are not available. First, an MRI close in size to the participant's head and demographic characteristics can be selected from a freely available MRI database (e.g., the Neurodevelopmental MRI Database; Richards et al., 2015b; Richards and Xie, 2015). This solution requires collecting precise head measures of the participant's head to find the ideal match within a set of MRIs. We recommend obtaining multiple head measures, in order to obtain a description of the complex head shape as accurately as possible. A schematic representation of the head measurements is represented in Fig. 3. A flexible non-stretchable measuring tape and head calipers could be used to obtain accurate measures of the head circumference, front-to-back distance, and side-to-side distance. Second, an alternative option to the individual MRI is the use of age-appropriate average templates. MRI templates are constructed using acquisitions from a number of subjects. It is critical for developmental studies that the selected MRI template includes participants within the age range under investigation to capture appropriate features of the developing brain. Therefore, an age-appropriate average template can be utilized as a surrogate MRI for the head model construction, even in absence of the participant's head measures.

2.2. Electrode locations

An accurate co-registration of electrode positions with the MRI volume is an important requirement for realistic head models (Wang and Gotman, 2001). Average electrode locations do not reflect the actual net placement because of idiosyncratic differences in the participants' head shape, especially in infancy and childhood. Therefore, localizer systems should be implemented to define the analytical position of the electrodes on the scalp (Richards et al., 2015a). Many devices use different approaches to locate the electrodes in 3D space on the participant's head, e.g., electromagnetic field (e.g., 3-Space Fastrak-Polhemus, Colchester, VT, USA) or pictures (Geodesic Photogrammetry System (GPS), EGI, Inc.; Russell et al., 2005). In absence of a localizer system, pictures of the participant's net placement can be utilized to locate the electrodes in 3D space. The position of a few electrodes around the head can be utilized as fiducial markers for the reconstruction of all electrode placements. We suggest the use of 5 fiducial markers corresponding to the vertex, nasion, inion, and left and right preauricular, respectively Cz, 17, 75, 57, and 100 electrodes on the Hydrocel Geodesic Sensor Net (HGSN) 128-channel net. Pictures of the net placement may be taken to locate the fiducial markers on the participant's head, and manually placed on the MRI. The coordinates of the fiducial points are utilized to reconstruct the position of the remaining electrodes and co-registered to the MRI head. In Fig. 4

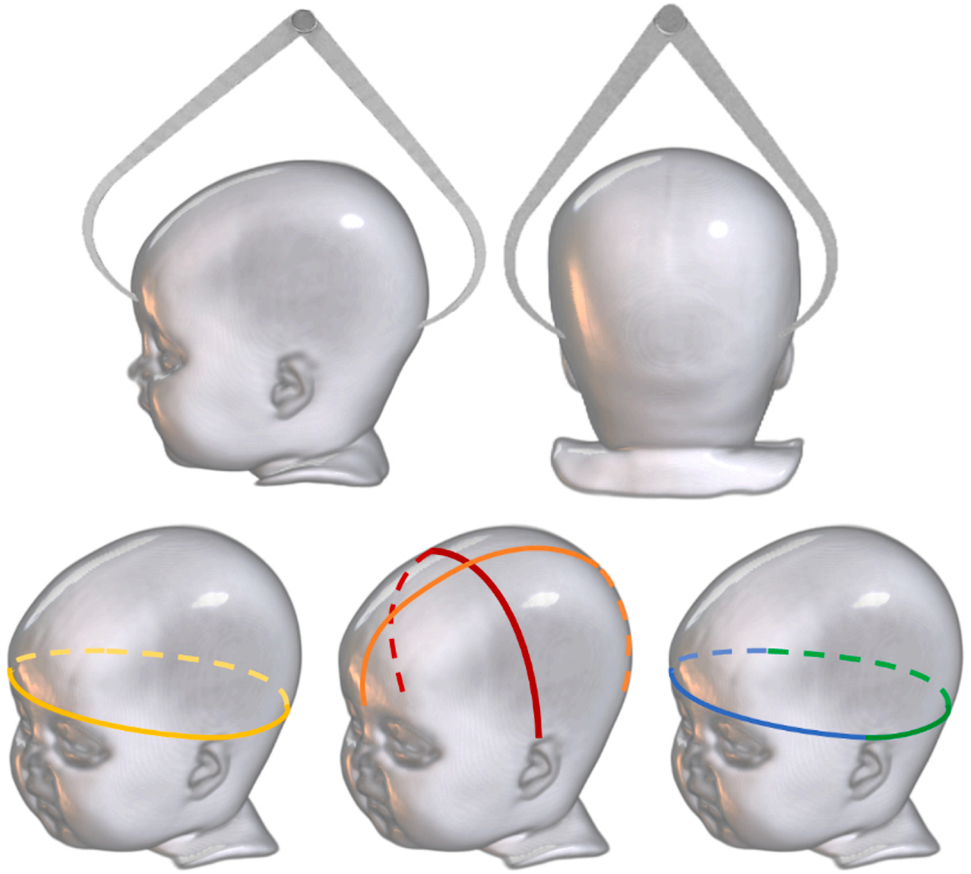

Fig. 3. Schematic illustration of the head measures to select the close in size MRI. Head width and length could be obtained through the use of a caliper (top panels). Head circumference (yellow line), sagittal (orange line), coronal (red line), and the frontal (blue line) and rear (green) semi-circumference measures may be obtained with a flexible tape.

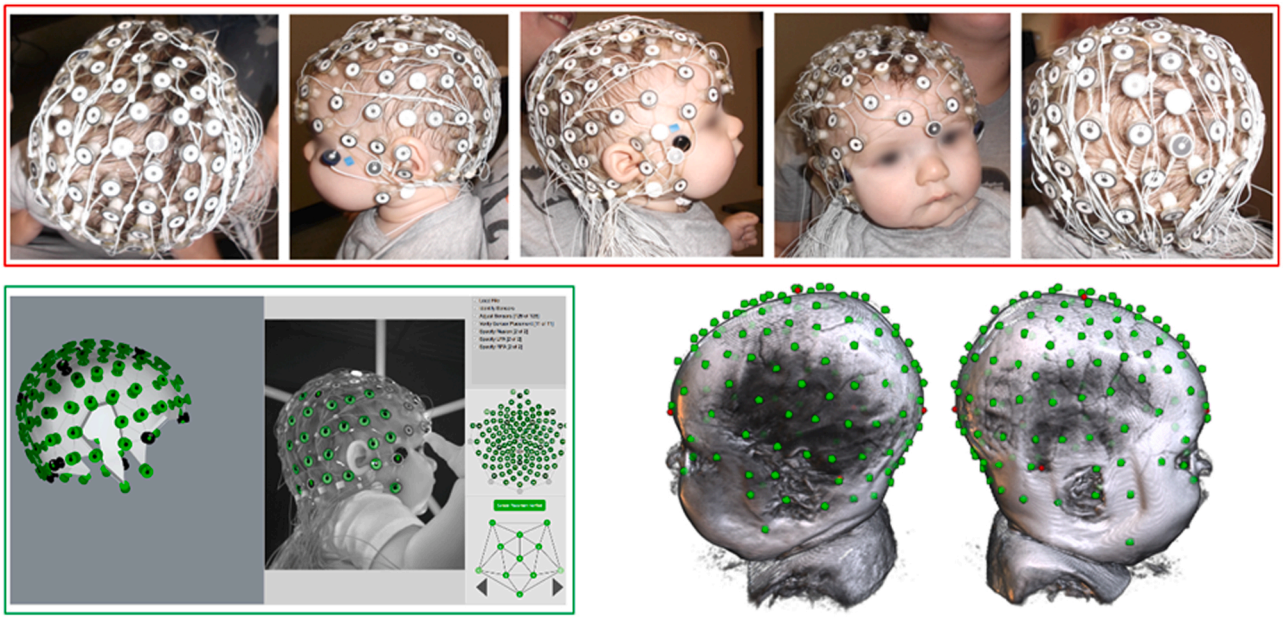

Fig. 4. 3D rendering view of the electrode location co-registered to the individual MRI (bottom right panel). Participant-specific electrode locations can be determined from pictures of the net placement (red box and electrodes) or from a digitalized representation of all electrode placements (green box and electrodes).

we provide an example of the pictures used for marking fiducials on an individual MRI and the HGSN 128-channel positions calculated with the Photogrammetry system co-registered to the MRI head volume. Additional work is necessary to perform quantitative comparisons between the alternative solutions to the electrodes' placements.

2.3. Head model construction

The forward solution in source analysis is obtained through the lead field matrix. The lead field matrix is calculated based on the source model, the head model, and the electrode placements (Fig. 1). The head model describes the head geometry and conductivity values of the considered compartments. Individualized head models come from an accurate segmentation of participants' MRIs and the use of age-appropriate conductivity values (Azizollahi et al., 2016). Several simulation studies have been conducted to define the effect of the head model on the accuracy of source localization (Conte and Richards, 2021a, 2021b; Hallez et al., 2007; Michel et al., 2004; Vorwerk et al., 2014). The main conclusions are that realistic head models should be preferred over simplified representations of the head (e.g., three-compartment concentric spheres) and at least five compartments should be modeled (i.e., skin, skull, CSF, GM, and WM; Conte and Richards, 2021a, 2021b; Vorwerk et al., 2018). In young infants, the exclusion of the CSF compartment from the head model has a bigger impact than the GM/WM distinction, and the exclusion of the fontanelles has produced local imprecisions in the source localization of areas underneath the fontanelles (Azizollahi et al., 2016).

Additional consideration should be given to the determination of conductivity values for the different compartments modeled for source localization. Age changes in tissue conductivity occur due to the different compositions of the different head media. High variability has been reposted in the estimation of brain-to-skull conductivity ratio in adults and young children, whereas a relatively consistent conductivity has been reposted for the remaining tissues. The skull compartment undergoes important changes due to its progressive ossification. Furthermore, the conductivity of the skull compartment in infancy is not uniform across its surface due to the presence of fontanelles, the closure of which does not complete until about 2 years of age (Duc and Largo, 1986). Several approaches have been implemented to estimate the best conductivity values for young children. For instance, Hämäläinen and colleagues (2011) fitted an exponential function to the available values in the literature to obtain an estimate of the skull conductivity for the age of interest (Hämäläinen et al., 2011).

A more recent approach tried to estimate the brain-to-skull conductivity ratio at the participant level via an iterative gradient-based approach based on near-dipolar EEG independent components defined by ICA (i.e., Simultaneous tissue Conductivity And source Location Estimation – SCALE; Akalin Acar et al., 2016a). The SCALE approach has been utilized with 12-month-old infant data and produced an estimation of conductivity ratio in the range of 9.8–12.1, suggesting a high inter-individual variability likely due to different maturational differences (Akalin Acar et al., 2016b). Further investigations need to be conducted to define the impact of inaccuracies in modeling conductivity values of the head tissue compartments on the localization of the electrical activity when important developmental structural changes occur.

Each medium in the FE method models can be represented with hexahedral or tetrahedral meshes. Both hexahedral and tetrahedral meshes perform well and show minimal differences in source analysis accuracy in studies with adult participants (Vorwerk et al., 2014, 2018; Wolters et al., 2007). Computational factors may be considered when deciding for the type of mesh to create. The tetrahedralization process is more complex and time consuming than hexahedral models generated directly from the MRI segmentation process. Here, we differentiate in our head models 10 different compartments (i.e., scalp, skull, dura, muscle, eyes, nasal cavity, CSF, GM, WM, and non-myelinated axons) and report source results obtained with both mesh types. A representation of the head model with hexahedral and tetrahedral meshes is reported in Fig. 5.

Lastly, a numerical solution to the forward problem needs to be incorporated when realistic head models are considered. Different methods have been proposed for the forward problem solution (Hämäläinen and Sarvas, 1989; Vatta et al., 2009; Vorwerk et al., 2017; Wolters et al., 2007). The most commonly used methods are the boundary element (BE) and finite element (FE). The former is usually implemented in models with hierarchical compartments, while the latter is used for more complex head geometries and it has been shown to achieve higher numerical accuracy (Vorwerk et al., 2018). FE models may be especially important for infants as they allow the identification of intraventricular CSF, which is not possible in BE compartment models (Conte and Richards, 2021a, 2021b).

2.4. Lead field and inverse solution

Electrode locations and head models are mathematically expressed

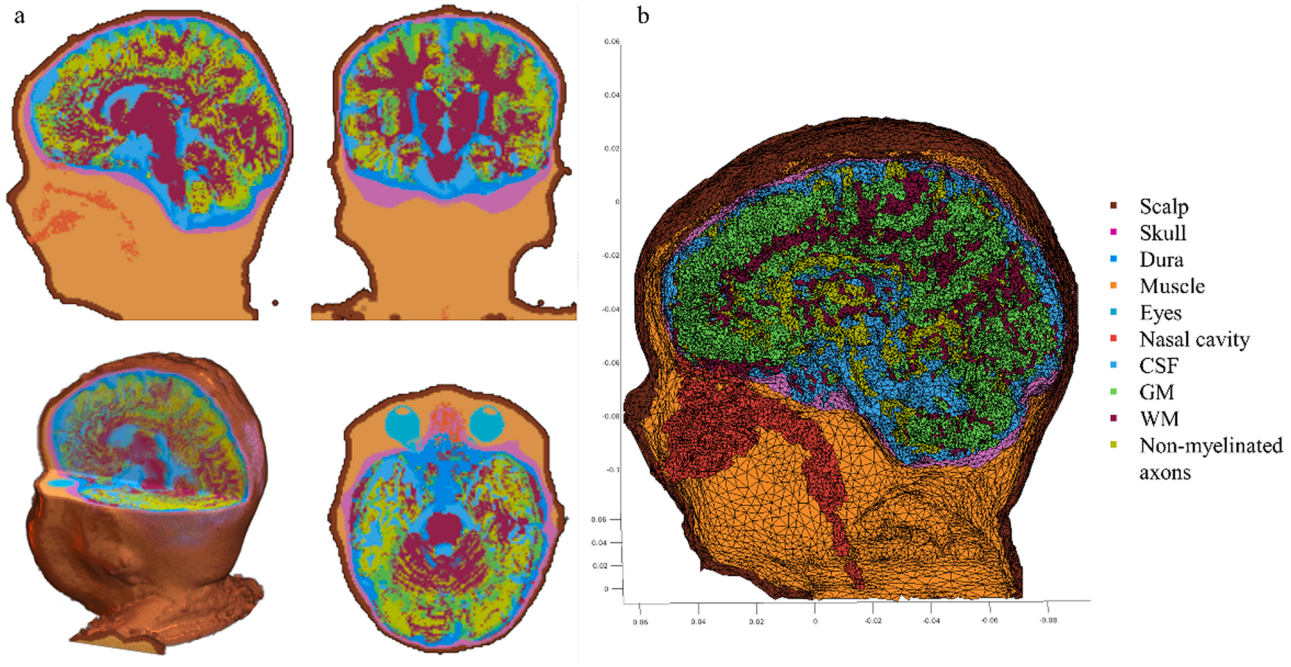

Fig. 5. Individual MRI segmentation output represented with hexahedral (panel a) and tetrahedral (panel b) meshes.

with the lead field matrix, which is used to solve the forward problem (for a review, see Hallez et al., 2007). The potentials at the electrodes are calculated based on the head model configuration. The sources that can explain the measured signal are reconstructed in source analysis (for a review, see Grech et al., 2008). The inverse problem occurs because of the ill-posed relation between electrodes and the inverse source model, i.e., few electrodes record the activity coming from several sources. There are a number of suggested inverse method procedures (e.g., minimum norm estimation; LORETA; sLORETA; eLORETA; for a review, see Grech et al., 2008). We use a distributed source analysis approach that does not require an assumption on the number of dipoles; the source space is created by using a realistic head model, derived from MRI (Dale et al., 1999); the eLORETA method (Pasqual-Marqui, 2007) is used as the restriction for the inverse problem; we use the GM and eyes as the source model (i.e., source grid in Fig. 2) with a 2 mm resolution for the hexahedral solution.

2.5. Source estimation

The source activation is represented in each voxel of the source space with a vector composed of three parameters, one per dimension in the space. The current density reconstruction (CDR) is then reduced to a single value by calculating the magnitude of the 3-dimensional vector (here referred to as the CDR approach) at each voxel location. Following this approach, high values in the original EEG data result in high CDR values, regardless of the polarity in the EEG signal. Alternatively, the singular value decomposition (SVD) can be utilized as a projection method. Differently from the CDR method, the polarity of the EEG activity is preserved in the reconstructed source. The SVD approach has been suggested to provide robust results in ERP source analysis and advantages in studies performing time-frequency decompositions and connectivity analysis (Rubega et al., 2019).

2.6. Study-specific atlas

The estimation of the current density is meaningful in a cluster of connected voxels covering some anatomical regions of interest (ROIs). Therefore, the source solution obtained across all voxels in the brain can be reduced to reflect the activity of a smaller number of ROIs. Study-specific atlases can be generated by registering existing stereotaxic atlases (e.g., Fillmore et al., 2015; Fonov et al., 2011; Oishi et al., 2019; Shi et al., 2011) to each participant and selecting specific ROIs. Alternatively, functional areas resulting from fMRI studies can be translated into binary representations of ROIs. A reduction of the voxel-wise source solution is performed by averaging the activity within the cluster of voxels comprising each ROI. This approach has the advantage of improving the signal-to-noise ratio within each ROI and reducing the number of statistical comparisons that could lead to family-wise error rates. The resulting output would consist of the source activity – expressed as CDR or SVD values – of each experimental condition and ROI.

The specifications for and results from one EEG recording from a 6-month-old infant are provided in the following sections. The EEG, MRI, and source analysis files contributing to this example may be accessed at https://osf.io/knf9t/. Results are reported for source analysis procedures performed on the participant's MRI, close MRI, and age-appropriate MRI template. Moreover, we presented the aggregate results of five 12-month-old infants who were part of a larger study investigating the neural correlates of face processing. These results were obtained through source analysis using only the age-appropriate MRI template.

3. Materials and methods

3.1. Participants and experimental procedure

Data were collected from one 6-month-old infant (M, 186 days). Aggregated results are reported for a representative group of five 12-month-old infants (1 male, M age = 376.4 days). All infants were full-term (at least 38 weeks gestation, birth weight at least 2500 g) and healthy at birth with no known developmental anomalies. Participants were primarily Caucasian and of middle socioeconomic status. Informed parental consent was obtained in accordance with ethics approval from the Institutional Review Board of the University of South Carolina.

All infants passively viewed upright, and inverted faces and houses presented for 500 ms in random order without replacement. A variable inter-trial interval was utilized for the sequence of stimuli and Sesame Street videos were presented as attention-getters when infants looked away from the screen. Further details about the EEG procedure can be found in Conte et al. (2020). Head measurements were taken before the beginning of the EEG task. Pictures and electrode positions via the GPS (see Fig. 4) were taken at the end of the EEG task.

3.2. EEG data acquisition

Participants were fitted with a 128-channel HGSN matching the infant's head circumference. The EEG was recorded from 124 channels in the electrode net and two channels over the outer canthi for electrooculogram (EOG). Impedances were kept below 100 kΩ and a 0.1–100 Hz band-pass filter was applied during the recordings. The vertex-referenced EEG was algebraically recomputed to an average reference. The EEG recordings were processed with the EEGLAB (version 14.1.1b) and ERPLAB toolboxes (Delorme and Makeig, 2004; Lopez-Calderon and Luck, 2014) within MATLAB R2019a. Channels with EEG artifacts were identified through an automatic procedure and visual inspection and substituted with data from the five closest electrodes. Trials with 12 or more bad channels were rejected. Details about the EEG preprocessing procedures can be found in Conte et al. (2020). An average of 46 good trials were considered for the 6-month-old participant (upright face $N = 43$, inverted face $N = 43$, upright house $N = 48$, inverted house $N = 50$). The group of 12-month-old infants had on average 31 good trials (upright face $M = 30$, inverted face $M = 31$, upright house $M = 30$, inverted house $M = 31$).

3.3. MRI data acquisition and preprocessing

The participant's MRI volume was collected in a separate session on a Siemens Magnetom Prisma 3.0 T scanner (Siemens, Erlangen, Germany) with a 20-channel head coil. Whole-head T1-weighted images were acquired with an MP-RAGE protocol using the following parameters: repetition time (TR) = 3000 ms, echo time (TE) = 4.44 ms, flip angle (FA) = 9°, field of view (FoV) = 192 × 192 pixels, voxel size = 1.0 × 1.0 × 1.0 mm. The total acquisition time was 9 min and 36 s. T2-weighted images were acquired using an SPC sequence lasting for 4 min and 32 s (TR = 4500 ms, TE = 13 ms, FoV = 192 ×192 pixels, voxel size = 1.0 ×1.0 ×2.5 mm). A realistic head model was obtained from the segmentation of the MRI into 10 different tissue types (Fig. 5). Conductivity values of each tissue type were as follow: scalp 0.35 S/m, skull 0.0132 S/m, CSF 1.79 S/m, WM 0.2 S/m, GM 0.33 S/m, dura 0.33 S/m, muscles 0.35 S/m, eyes 0.5 S/m, and nasal cavity 0.0048 S/m. Details about the segmenting procedure can be found elsewhere (Gao et al., 2019; Richards, 2013).

Anatomical ROIs were defined based on anatomical stereotaxic atlases (Fillmore et al., 2015; Gao et al., 2019; Guy et al., 2016; Heckemann et al., 2003, 2006; Shattuck et al., 2008). These atlases were used to define 17 anatomical areas of interest to the hypothesis about the neural source of face processing in infants (Conte et al., 2020; Guy et al., 2016). A 3D rendering representation of the selected ROIs is reported in Fig. 6.

4. Results

The ERP activity of the representative 6-month-old participant is

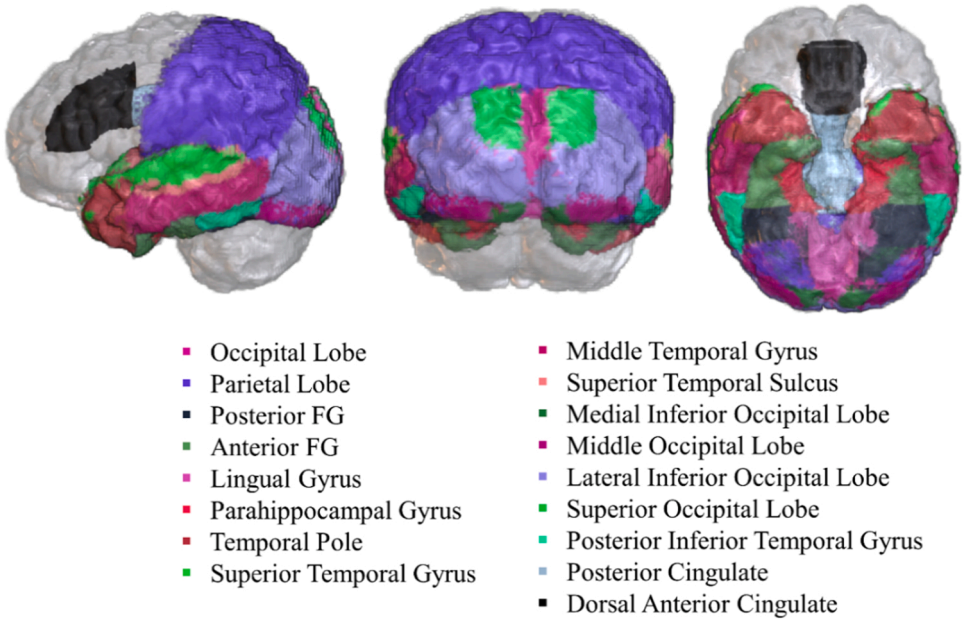

Fig. 6. The subset of anatomical areas defined from different atlases (LONI Probabilistic Brain Atlas, LPBA; Hammers atlas of MRIs from the IXI project). Each atlas was registered to the 6-month-old's MRI. Occipitotemporal and parietal areas of interest were selected.

represented in Fig. 7 as a function of stimulus type (i.e., upright and inverted faces and houses) over parietal and parieto-occipital channels of the 10–10 system (i.e., P7–10 and PO7–10). For the purpose of the current work, we will focus on the P400 ERP component. The P400 ranged from about 400–600 ms after stimulus onset and was of larger amplitude over right-lateralized electrodes (e.g., P10 and PO10). Similarly, the scalp maps showed larger and right-lateralized activity in response to faces than houses.

The estimated source was computed at each point of the source grid, here constrained to the GM and eyes. The inverse solution was then applied to the data and calculated as CDR and SVD values at each point of the grid. The dimensions of the resulting 3D matrix were defined by the number of points in the grid, number of conditions, and number of time points. *ApplyInverse.m* applies the inverse solution to the ERP data and calculates either the CDR or SVD values based on the user's preference. A detailed description of the script is reported in the README document at https://osf.io/knf9t/. The resulting 3D matrix may be saved for visualization purposes. *PlotSource.m* applies interpolation functions to the source solution (i.e., 3D matrix) and saves the source output as a NIfTI image (for details, see README https://osf.io/knf9t/).

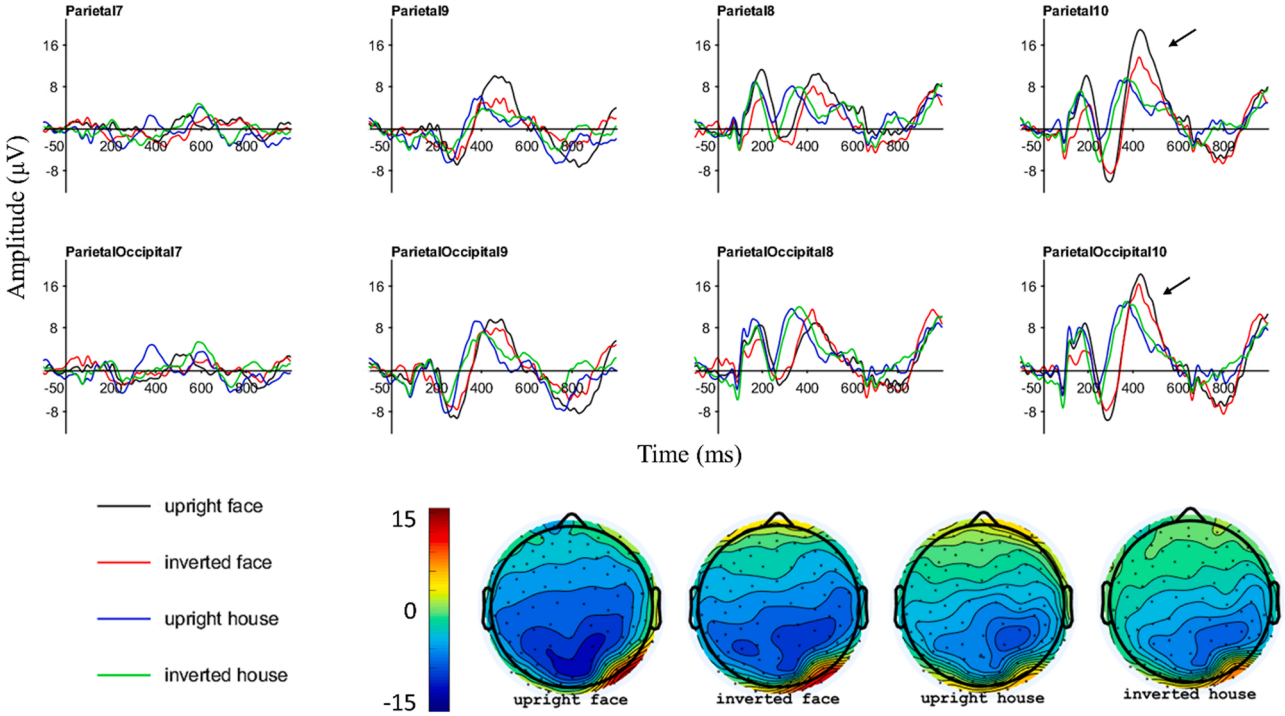

Fig. 7. ERP line plots of a representative 6-month-old infant over parietal and parietal-occipital channels. The ERP activity of the whole segment is plotted as a function of stimulus type (top panels). The scalp maps show the activity at the peak of the P400 component (i.e., 432 ms after stimulus onset) for all stimulus types.

A specific set of ROIs can be applied to the reconstructed source activity and used for further analyses. The ROI set can be created from existing stereotaxic atlases or the subject's functional response in fMRI tasks. *ApplyROIfilter.m* reduces the source solution to the selected ROIs and computes the mean activity for each area of interest. The final solution is expressed as a 3D matrix with the number of ROIs, number of conditions, and number of time points. Results of the distributed activity at the P400 peak in response to upright faces are reported in Fig. 8 as 3D rendering plots. Line plots report the source activity for the four experimental conditions in specific ROIs. The activity in both the superior temporal sulcus and posterior cingulate resembled the ERP pattern of response. In the 400–600 ms time window the response to faces was larger than the response to houses. There seemed to be a face-specific inversion effect at the peak of the reconstructed P400 ERP.

Similar solutions were obtained by using both an MRI close in size to the participant's head and the age-appropriate MRI template. Results for the hexahedral meshes are reported in Fig. 9.

In Fig. 10 we compared the source activity in the posterior cingulate obtained from the three different head models. The patterns of response were similar for the three solutions. The results from the self and close MRIs were more similar to each other than the result obtained with the age-appropriate MRI for the grand average data across conditions. However, only the self- and close-MRI solutions seemed to be sensitive to the face-inversion effect. These results should be further explored in studies with larger sample size. All in all, source analyses procedures performed using head models tailored to the participants' head features and electrode locations would provide more accurate solutions. Nonetheless, source solutions obtained with age-appropriate head models are to be considered more appropriate than the use of adult head models.

Lastly, we applied the source analysis procedure to a small group of 12-month-old participants using an age-appropriate MRI template and hexahedral meshes for the head model. Forward and inverse solutions were applied at the participant level, and the resulting output was averaged across participants. Aggregated results for both the ERP and CDR values are depicted in Fig. 11.

5. Discussion

We provided an overview of the procedure for EEG source analysis with particular reference to the adjustments necessary to perform such analyses with data acquired from pediatric populations. Critical aspects for EEG source reconstruction are obtaining an accurate map of electrode locations and a realistic head model. A digital map of all electrode locations (i.e., GPS solution) is the most accurate way to obtain 3D coordinates of all electrodes with a procedure that is tolerated by very young infants. Alternatively, digital coordinates of a few fiducial electrodes can be used to reconstruct the location of the remaining positions. Fiducial electrodes can be manually placed on an MRI by trained researchers using pictures of the participant's EEG net placement when digitalized electrode or fiducial positions are not available. We recommend that pictures are taken from all head sides (see Fig. 4) at the end of the EEG session. All these alternative solutions for electrode placement provide realistic coordinates that take into account individual differences in head shape and net placement. Individualized electrode placements are to be preferred to standard electrode locations coming from adult studies (Richards et al., 2015a) in order to reduce source localization errors (Wang and Gotman, 2001).

The head model construction is another critical step in source analysis studies. The use of realistic head models is advantageous in minimizing the source localization error regardless of the age group under investigation (Vorwerk et al., 2014). However, the scarcity of pediatric MRIs and MRI templates has led developmental researchers to use adult head models (Albrecht et al., 2000; van Leeuwen et al., 2007). Such an approach increases the localization errors given the anatomical differences across participants of different ages. An optimal solution would consist of the use of individual MRIs from which the head model is

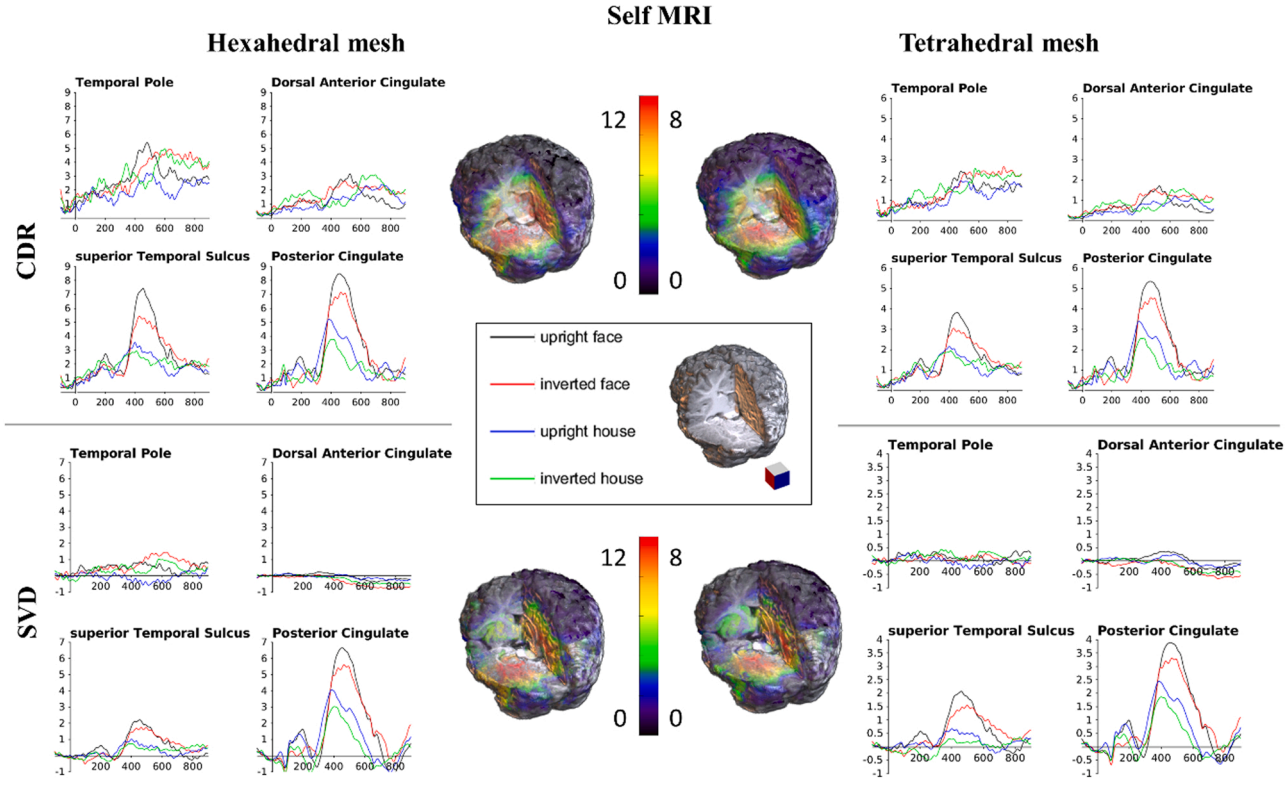

Fig. 8. The activity in response to upright faces at the peak of the P400 ERP (i.e., 432 ms) is plotted on the individual T1-weighted MRI. (a) Reconstructed source activity using the individual head model reported for the two mesh types (hexahedral, tetrahedral) and source measures (CDR, SVD). (b) Line plots depict the source activity throughout the trial duration for the four experimental conditions.

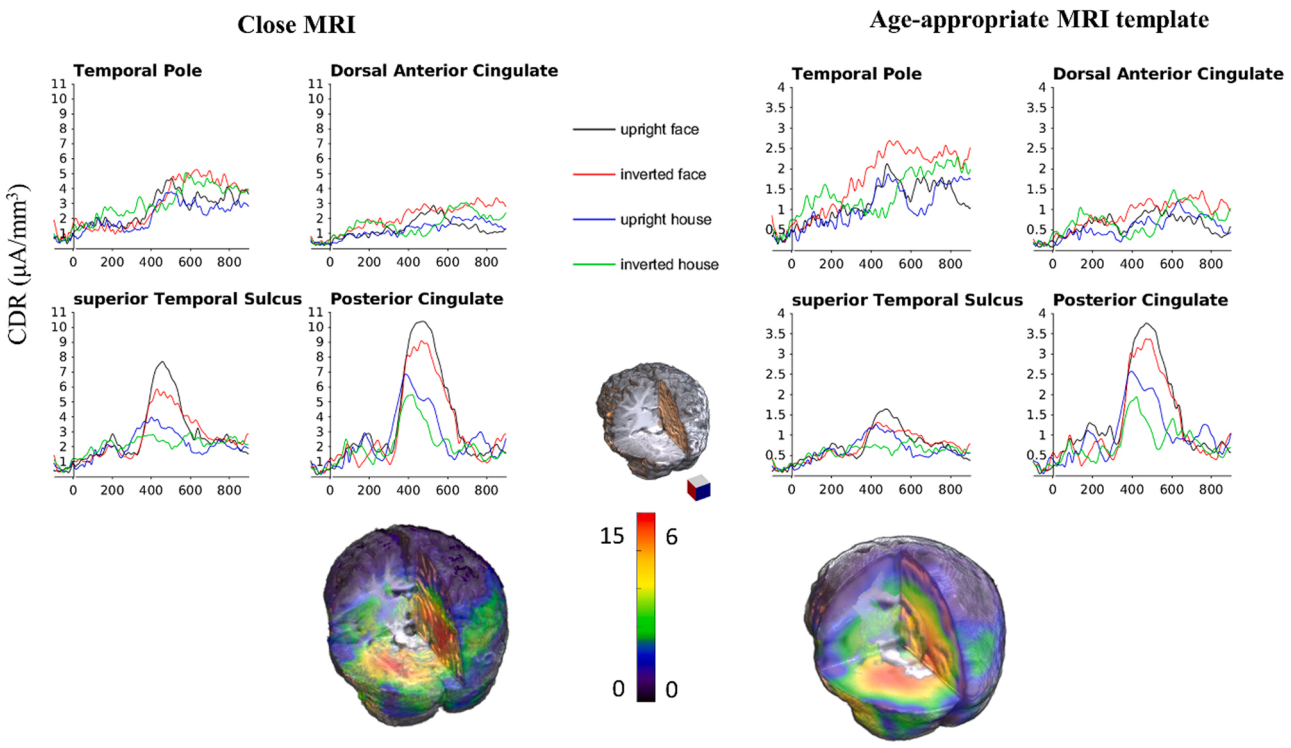

Fig. 9. (a) Line plots and 3D renderings of the source analysis results obtained from the close-MRI head model (left panels) and the average-template head model (right panels). (b) The 3D rendering plots show the reconstructed source in response to faces at the P400 peak plotted on the close or age-appropriate T1-weighted MRI. (c) Line plots show the source activity for the four experimental conditions.

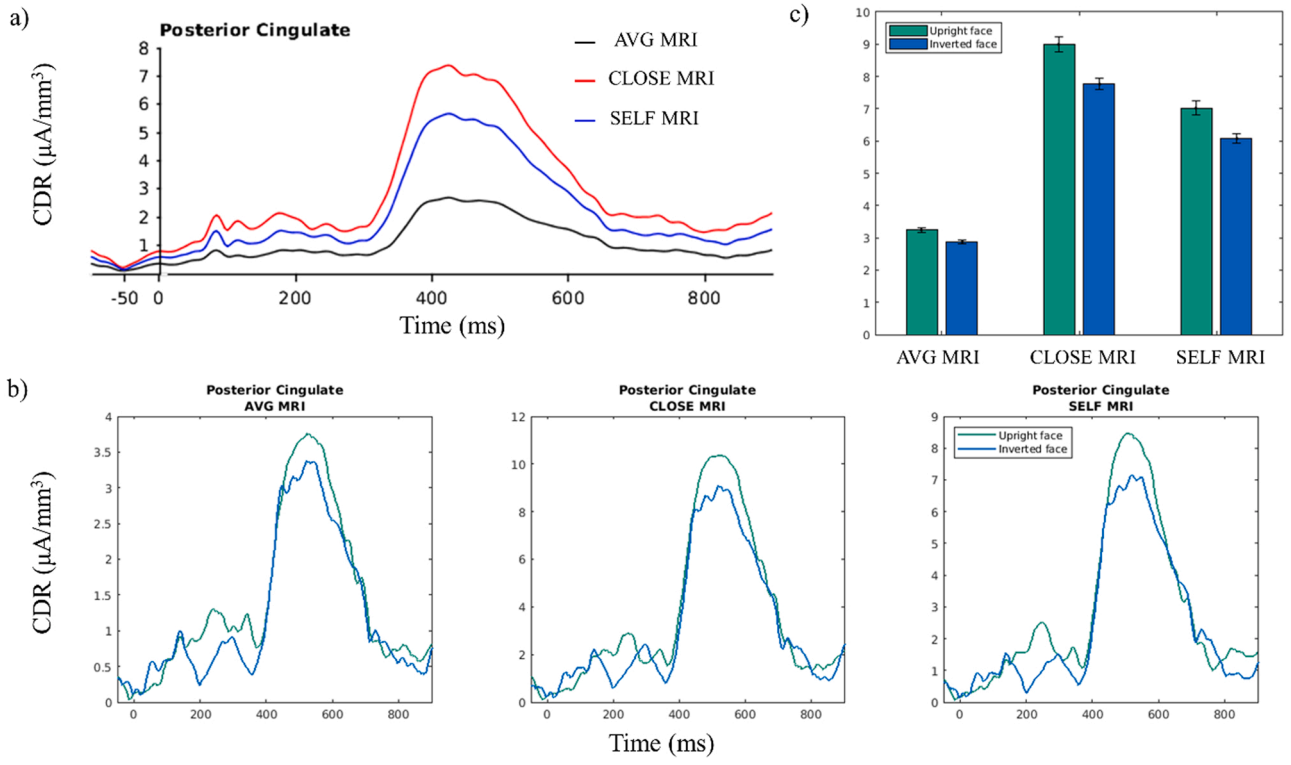

Fig. 10. CDR activity in the posterior cingulate as a function of MRI type (panel a) and face orientation (panel b) for a representative participant. Note that the y-axis scale is set to maximize each distribution. The average amplitude between 400 and 600 ms is plotted as a function of face orientation (panel c; error bars represent the standard error of the mean). The face inversion effect within the P400 time window seems to be more pronounced when either a self or close MRI is used.

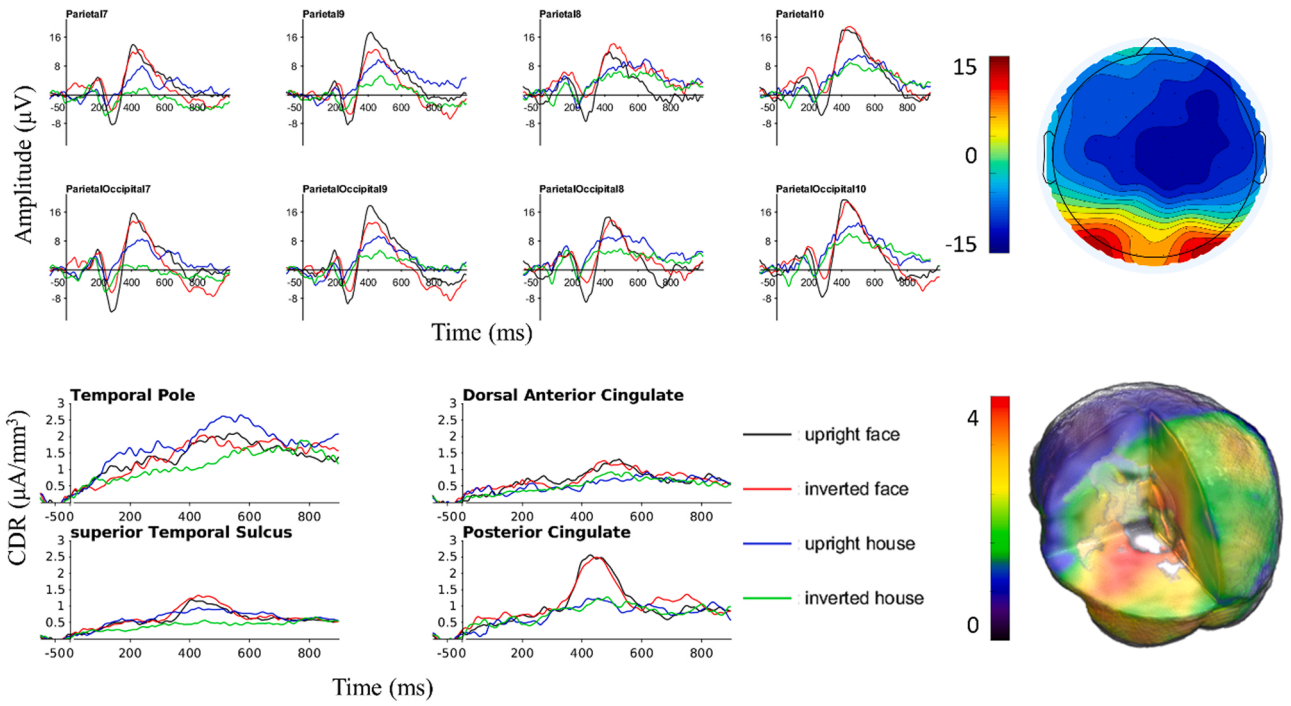

Fig. 11. Aggregated data from a small sample of 12-month-old participants. Top panels report the ERP response over parietal and parietal occipital channels for the four experimental conditions, along with the scalp map at the P400 peak (i.e., 400 ms after stimulus onset) for upright faces. Bottom panels show the CDR activity in four ROIs as a function of stimulus type and the 3D rendering of the voxel-wise source map for upright faces at the P400 peak.

defined. However, the acquisition of individual MRI volume is not always feasible, especially with very young participants, because of practical and technical challenges that characterize the acquisition protocol for pediatric age groups.

One solution would be to select for each participant an MRI volume from a large set of volumes included in imaging databases. The volume would match the participant's head size and demographic characteristics (e.g., age, biological sex). To this end, it is pivotal that accurate head measurements are taken during the experimental session. Age-appropriate MRI templates may be used when head measurements are not available. The same head model and source space are used for all participants to calculate the neural generator(s) of the scalp EEG activity. Thus, potential individual differences may be overlooked and result in an increase in localization error. However, small localization errors coming from the use of average templates for the head model construction can be compensated by averaging the source activity within pre-defined anatomical ROIs. Results from our comparisons with one representative participant suggest that similar source activation patterns in the posterior cingulate result from age-appropriate head models in the form of self MRI, close MRI, or MRI template. Further research is necessary to better quantify the localization errors generated with the three alternative head model solutions (Fu and Richards, 2022).

An additional challenge in the head model construction is defining the number of different tissues to model. Findings from adult studies using both simulation and experimental approaches seem to suggest the critical role of modeling the CSF in the head volume conductor. Neglecting or misidentifying the CSF has a negative impact on both signal topography and magnitude (Conte & Richards, 2021a; Bangera et al., 2010; Vorwerk et al., 2014). Although not yet empirically tested, it is plausible to believe that modeling the CSF would be even more important for developmental studies given the larger amount of this highly conductive compartment in young participants than adults. The distinction between GM and WM, and the inclusion of WM anisotropy values from diffusion-weighted imaging volumes seem to be important for accurate head modeling. The greatest improvement from anisotropic models is obtained for sources close to a region with high anisotropy (Bangera et al., 2010), while it has only a marginal influence for sources far from regions with high anisotropy (Vorwerk et al., 2014). The variability in the amount of WM myelination in pediatric populations, both within participants of the same age and across age groups, may make the modeling of WM anisotropy critical for improving source localization accuracy in developmental research.

A final highly debated topic is the use of BE or FE approaches to the EEG forward problem. Historically, BE forward methods relied on approximate and simplified head representations obtained by modeling three nested compartments (i.e., skin, skull, brain) with isotropic conductivity. Higher numerical accuracies can be obtained from realistic three-compartment models using the BE approach. Nonetheless, FE methods are able to handle both complex geometries that model non-nested compartments (e.g., the CSF) and anisotropy (e.g., in the GM and WM compartments). Thus, FE methods may be a preferable solution for source analysis with pediatric datasets.

In summary, the gold standard approach for source analysis utilizes digital maps of electrode locations and individualized head models from the participant's MRI. Alternative approaches can be implemented to overcome the limitation of obtaining the electrode placements and MRI for each participant. A map of the electrode coordinates can be reconstructed from the coordinates of a few electrode markers using either a neuronavigation system or pictures of the net placement. An MRI close in size to the participant's head or an age-appropriate MRI template can be utilized to create the head and source models. We provided two scripts for applying the inverse model to EEG data and performing ROI calculations. In the examples described here, we applied the scripts to ERP datasets but similar results can be obtained with segmented, non-aggregated data (i.e., epoched EEG datasets). EEG input data should be preferred for studies including time-frequency or connectivity analyses. These advanced EEG calculations that include nonlinear data transformations can be performed voxel-wise using CDR/SVD values. Moreover, we performed source analysis on 2 mm grids using both hexahedral and tetrahedral meshes and calculated the inverse solution via eLORETA. Different source spaces and inverse models may be utilized as input for the current density reconstruction. Similarly, study-

specific ROI atlases can be used as inputs in the ROI filter script. All scripts are freely available under Creative Commons Attribution 4.0 International Public License and may be accessed at https://osf.io/knf9t/.

Declaration of Competing Interest

The authors declare that they have no known competing financial interests or personal relationships that could have appeared to influence the work reported in this paper.

Acknowledgments

This research was supported by grants from the National Institute of Child Health and Human Development (NICHD) of the National Institute of Health under award numbers K99HD102566 to Dr. Conte, and R01HD18942 to Dr. Richards.

References

Albrecht, R., Suchodoletz, W. v, Uwer, R., 2000. The development of auditory evoked dipole source activity from childhood to adulthood. Clin. Neurophysiol. 111 (12), 2268–2276. https://doi.org/10.1016/S1388-2457(00)00464-8.

Acar, Z.A., Acar, C.E., Makeig, S., 2016a. Simultaneous head tissue conductivity and EEG source location estimation. NeuroImage 124, 168–180. https://doi.org/10.1016/j.neuroimage.2015.08.032.

Acar, Z.A., Ortiz-Mantilla, S., Benasich, A., Makeig, S., 2016b. High-resolution EEG source imaging of one-year-old children. 2016 38th Annual International Conference of the IEEE Engineering in Medicine and Biology Society (EMBC). IEEE,, pp. 117–120. https://doi.org/10.1109/EMBC.2016.7590654.

Azizollahi, H., Aarabi, A., Wallois, F., 2016. Effects of uncertainty in head tissue conductivity and complexity on EEG forward modeling in neonates. Hum. brain Mapp. 37 (10), 3604–3622.

Azizollahi, H., Aarabi, A., Wallois, F., 2020. Effect of structural complexities in head modeling on the accuracy of EEG source localization in neonates. J. Neural Eng. 17 (5) https://doi.org/10.1088/1741-2552/abb994.

Bangera, N.B., Schomer, D.L., Dehghani, N., Ulbert, I., Cash, S., Papavasiliou, S., Halgren, E., 2010. Experimental validation of the influence of white matter anisotropy on the intracranial EEG forward solution. J. Comput. Neurosci. 29 (3), 371–387. https://doi.org/10.1007/s10827-009-0205-z.

Beauchamp, M.S., Beurlot, M.R., Fava, E., Nath, A.R., Parikh, N.A., Saad, Z.S., Oghalai, J. S., 2011. The developmental trajectory of brain-scalp distance from birth through childhood: implications for functional neuroimaging. PloS One 6 (9), e24981. https://doi.org/10.1371/journal.pone.0024981.

Buzzell, G.A., Richards, J.E., White, L.K., Barker, T.V., Pine, D.S., Fox, N.A., 2017. Development of the error-monitoring system from ages 9–35: Unique insight provided by MRI-constrained source localization of EEG. NeuroImage 157, 13–26. https://doi.org/10.1016/j.neuroimage.2017.05.045.

Cantiani, C., Ortiz-Mantilla, S., Riva, V., Piazza, C., Bettoni, R., Musacchia, G., Benasich, A.A., 2019. Reduced left-lateralized pattern of event-related EEG oscillations in infants at familial risk for language and learning impairment. NeuroImage: Clin. 22, 101778 https://doi.org/10.1016/j.nicl.2019.101778.

Conte, S., Richards, J.E., 2021a. The Influence of the Head Model Conductor on the Source Localization of Auditory Evoked Potentials. Brain Topogr. 1–20. https://doi.org/10.1007/s10548-021-00871-z.

Conte, S., Richards, J.E. (2021b). *The Influence of the Head Model in EEG Source Localization with Infants*. Manuscript in preparation.

Conte, S., Richards, J.E., Guy, M.W., Xie, W., Roberts, J.E., 2020. Face-sensitive brain responses in the first year of life. NeuroImage *211*. https://doi.org/10.1016/j.neuroimage.2020.116602.

Crouzeix, A., Yvert, B., Bertrand, O., Pernier, J., 1999. An evaluation of dipole reconstruction accuracy with spherical and realistic head models in MEG. Clin. Neurophysiol. 110 (12), 2176–2188. https://doi.org/10.1016/S1388-2457(99)00174-1.

Dale, A.M., Fischl, B., Sereno, M.I., 1999. Cortical surface-based analysis: I. Segmentation and surface reconstruction. NeuroImage 9 (2), 179–194. https://doi.org/10.1006/nimg.1998.0395.

Debnath, R., Buzzell, G.A., Morales, S., Bowers, M.E., Leach, S.C., Fox, N.A., 2020. The Maryland analysis of developmental EEG (MADE) pipeline. Psychophysiology 57 (6). https://doi.org/10.1111/psyp.13580.

Delorme, A., Makeig, S., 2004. EEGLAB: an open source toolbox for analysis of single-trial EEG dynamics including independent component analysis. J. Neurosci. Methods 134 (1), 9–21. https://doi.org/10.1016/j.jneumeth.2003.10.009.

Duc, G., Largo, R.H., 1986. Anterior fontanel: size and closure in term and preterm infants. Pediatrics 78 (5), 904–908. https://doi.org/10.1542/peds.78.5.904.

Ellis, C.T., Skalaban, L.J., Yates, T.S., Bejjanki, V.R., Córdova, N.I., Turk-Browne, N.B., 2021a. Evidence of hippocampal learning in human infants. Curr. Biol. 31 (15), 3358–3364. https://doi.org/10.1016/j.cub.2021.04.072.

Ellis, C.T., Skalaban, L.J., Yates, T.S., Turk-Browne, N.B., 2021b. Attention recruits frontal cortex in human infants. Proc. Natl. Acad. Sci. 118 (12) https://doi.org/10.1073/pnas.2021474118.

Ellis, C.T., Yates, T.S., Skalaban, L.J., Bejjanki, V.R., Arcaro, M.J., Turk-Browne, N.B., 2021c. Retinotopic organization of visual cortex in human infants. Neuron 109 (16), 2616–2626. https://doi.org/10.1016/j.neuron.2021.06.004.

Fillmore, P.T., Richards, J.E., Phillips-Meek, M.C., Cryer, A., Stevens, M., 2015. Stereotaxic magnetic resonance imaging brain atlases for infants from 3 to 12 months. Dev. Neurosci. 37 (6), 515–532. https://doi.org/10.1159/000438749.

Fonov, V., Evans, A.C., Botteron, K., Almli, C.R., McKinstry, R.C., Collins, D.L., 2011. Unbiased average age-appropriate atlases for pediatric studies. NeuroImage 54 (1), 313–327. https://doi.org/10.1016/j.neuroimage.2010.07.033.

Flemming, L., Wang, Y., Caprihan, A., Eiselt, M., Haueisen, J., Okada, Y., 2005. Evaluation of the distortion of EEG signals caused by a hole in the skull mimicking the fontanel in the skull of human neonates. Clin. Neurophysiol. 116 (5), 1141–1152. https://doi.org/10.1016/j.clinph.2005.01.007.

Gabard-Durnam, L.J., Mendez Leal, A.S., Wilkinson, C.L., Levin, A.R., 2018. The Harvard Automated Processing Pipeline for Electroencephalography (HAPPE): Standardized Processing Software for Developmental and High-Artifact Data. Front. Neurosci. 12, 97. https://doi.org/10.3389/fnins.2018.00097.

Gao, C., Conte, S., Richards, J.E., Xie, W., Hanayik, T., 2019. The neural sources of N170: Understanding timing of activation in face-selective areas. Psychophysiology. https://doi.org/10.1111/psyp.13336.

Gargiulo, P., Belfiore, P., Friðgeirsson, E.A., Vanhatalo, S., Ramon, C., 2015. The effect of fontanel on scalp EEG potentials in the neonate. Clin. Neurophysiol. 126 (9), 1703–1710. https://doi.org/10.1016/j.clinph.2014.12.002.

Grech, R., Cassar, T., Muscat, J., Camilleri, K.P., Fabri, S.G., Zervakis, M., Vanrumste, B., 2008. Review on solving the inverse problem in EEG source analysis. J. Neuroeng. Rehabil. 5, 1–33. https://doi.org/10.1186/1743-0003-5-25.

Guy, M.W., Zieber, N., Richards, J.E., 2016. The Cortical Development of Specialized Face Processing in Infancy. Child Dev. 87 (5), 1581–1600. https://doi.org/10.1111/cdev.1254.

Hallez, H., Vanrumste, B., Grech, R., Muscat, J., De Clercq, W., Vergult, A., Lemahieu, I., 2007. Review on solving the forward problem in EEG source analysis. J. Neuroeng. Rehabil. 4. https://doi.org/10.1186/1743-0003-4-46.

Hämäläinen, J.A., Ortiz-Mantilla, S., Benasich, A.A., 2011. Source localization of event-related potentials to pitch change mapped onto age-appropriate MRIs at 6months of age. NeuroImage 54 (3), 1910–1918. https://doi.org/10.1016/j.neuroimage.2010.10.016.

Hämäläinen, M.S., Sarvas, J., 1989. Realistic Conductivity Geometry Model of the Human Head for Interpretation of Neuromagnetic Data. IEEE Trans. Biomed. Eng. 36 (2), 165–171. https://doi.org/10.1109/10.16463.

Heckemann, R.A., Hajnal, J.V., Aljabar, P., Rueckert, D., Hammers, A., 2006. Automatic anatomical brain MRI segmentation combining label propagation and decision fusion. NeuroImage 33 (1), 115–126. https://doi.org/10.1016/j.neuroimage.2006.05.061.

Fu, X. & Richards, J.E. (2022). *Evaluating Head Models for Cortical Source Localization of the Face-Sensitive N290 Component in Infants*. [Manuscript submitted for publication].

Heckemann, R.A., Hartkens, T., Leung, K.K., Zheng, Y., Hill, D.L., Hajnal, J.V., & Rueckert, D. (2003). Information extraction from medical images: developing an e-Science application based on the Globus toolkit. In *Proceedings of the 2nd UK e-Science All Hands Meeting.*

Hendrix, C., Thomason, M.E., 2021. September 29 Protoc. Recomm. 54 Infant Toddler neuroimaging Res. Labs. https://doi.org/10.31234/osf.io/zktbg.

Izard, V., Dehaene-Lambertz, G., Dehaene, S., 2008. Distinct cerebral pathways for object identity and number in human infants. PLoS Biol. 6 (2), 0275–0285. https://doi.org/10.1371/journal.pbio.0060011.

Ladouceur, C.D., Dahl, R.E., Birmaher, B., Axelson, D.A., Ryan, N.D., 2006. Increased error-related negativity (ERN) in childhood anxiety disorders: ERP and source localization. J. Child Psychol. Psychiatry Allied Discip. 47 (10), 1073–1082. https://doi.org/10.1111/j.1469-7610.2006.01654.x.

Lew, S., Sliva, D.D., Choe, M.S., Grant, P.E., Okada, Y., Wolters, C.H., Hämäläinen, M.S., 2013. Effects of sutures and fontanels on MEG and EEG source analysis in a realistic infant head model. Neuroimage 76, 282–293. https://doi.org/10.1016/j.neuroimage.2013.03.017.

Lopez-Calderon, J., Luck, S.J., 2014. ERPLAB: an open-source toolbox for the analysis of event-related potentials. Front. Hum. Neurosci. 8, 213. https://doi.org/10.3389/fnhum.2014.00213.

Michel, C.M., Murray, M.M., Lantz, G., Gonzalez, S., Spinelli, L., Grave De Peralta, R., 2004. EEG source imaging. Clin. Neurophysiol. 115 (10), 2195–2222. https://doi.org/10.1016/j.clinph.2004.06.001.

Oishi, K., Chang, L., Huang, H., 2019. Baby brain atlases. January 15 NeuroImage. Academic Press Inc,. https://doi.org/10.1016/j.neuroimage.2018.04.003.

Ortiz-Mantilla, S., Hämäläinen, J.A., Benasich, A.A., 2012. Time course of ERP generators to syllables in infants: A source localization study using age-appropriate brain templates. NeuroImage 59 (4), 3275–3287. https://doi.org/10.1016/j.neuroimage.2011.11.048.

Pasqual-Marqui, R., 2007. Discrete, 3D distributed linear imaging methods of electric neuronal activity. Part 1: exact, zero error localization. Signal Process. 81, 855–879. https://doi.org/10.1016/j.neulet.2010.09.011.

Raschle, N., Zuk, J., Ortiz-Mantilla, S., Sliva, D.D., Franceschi, A., Grant, P.E., Gaab, N., 2012. Pediatric neuroimaging in early childhood and infancy: Challenges and practical guidelines. Ann. N. Y. Acad. Sci. 1252 (1), 43–50. https://doi.org/10.1111/j.1749-6632.2012.06457.x.

Reynolds, G.D., Richards, J.E., 2005. Familiarization, attention, and recognition memory in infancy: An event-related potential and cortical source localization study. Dev. Psychol. 41 (4), 598–615. https://doi.org/10.1037/0012-1649.41.4.598.
Reynolds, G.D., Richards, J.E., 2009. Cortical source localization of infant cognition. Dev. Neuropsychol. 34 (3), 312–329. https://doi.org/10.1080/87565640902801890.
Richards, J.E., 2005. Localizing cortical sources of event-related potentials in infants' covert orienting. Dev. Sci. 8 (3), 255–278. https://doi.org/10.1111/j.1467-7687.2005.00414.x.
Richards, J.E., 2013. Cortical sources of ERP in prosaccade and antisaccade eye movements using realistic source models. Front. Syst. Neurosci. 7 (July), 1–20. https://doi.org/10.3389/fnsys.2013.00027.
Richards, J.E., Boswell, C., Stevens, M., Vendemia, J.M.C., 2015a. Evaluating Methods for Constructing Average High-Density Electrode Positions. Brain Topogr. 28 (1), 70–86. https://doi.org/10.1007/s10548-014-0400-8.
Richards, J.E., Sanchez, C., Phillips-Meek, M., Xie, W., 2015b. A database of ageappropriate average MRI templates. Neuroimage. https://doi.org/10.1016/j.neuroimage.2015.04.055.
Richards, J.E., Xie, W., 2015. In: Bensen, J. (Ed.), Brains for all the ages: structural neurodevelopment in infants and children from a life-span perspective, vol. 48. Advances in Child Development and Beahvior.
Rubega, M., Carboni, M., Seeber, M., Pascucci, D., Tourbier, S., Toscano, G., Michel, C. M., 2019. Estimating EEG Source Dipole Orientation Based on Singular-value Decomposition for Connectivity Analysis. Brain Topogr. 32 (4), 704–719. https://doi.org/10.1007/s10548-018-0691-2.
Russell, G.S., Eriksen, K.J., Poolman, P., Luu, P., Tucker, D.M., 2005. Geodesic photogrammetry for localizing sensor positions in dense-array EEG. Clin. Neurophysiol. 116 (5), 1130–1140. https://doi.org/10.1016/j.clinph.2004.12.022.
Seeck, M., Koessler, L., Bast, T., Leijten, F., Michel, C., Baumgartner, C., Beniczky, S., 2017. The standardized EEG electrode array of the IFCN. Clin. Neurophysiol. 128 (10), 2070–2077. https://doi.org/10.1016/j.clinph.2017.06.254.
Sohrabpour, A., Lu, Y., Kankirawatana, P., Blount, J., Kim, H., He, B., 2015. Effect of EEG electrode number on epileptic source localization in pediatric patients. Clin. Neurophysiol. 126 (3), 472–480. https://doi.org/10.1016/j.clinph.2014.05.038.
Song, J., Davey, C., Poulsen, C., Luu, P., Turovets, S., Anderson, E., Tucker, D., 2015. EEG source localization: sensor density and head surface coverage. J. Neurosci. Methods 256, 9–21. https://doi.org/10.1016/j.jneumeth.2015.08.015.
Shi, F., Yap, P.T., Wu, G., Jia, H., Gilmore, J.H., Lin, W., Shen, D., 2011. Infant brain atlases from neonates to 1- and 2-year-olds. PLoS ONE 6 (4). https://doi.org/10.1371/journal.pone.0018746.
Shattuck, D.W., Mirza, M., Adisetiyo, V., Hojatkashani, C., Salamon, G., Narr, K.L., Toga, A.W., 2008. Construction of a 3D probabilistic atlas of human cortical structures. Neuroimage 39 (3), 1064–1080. https://doi.org/10.1016/j.neuroimage.2007.09.031.
Van Der Weel, F.R., Van Der Meer, A.L.H., 2009. Seeing it coming: Infants' brain responses to looming danger. Naturwissenschaften 96 (12), 1385–1391. https://doi.org/10.1007/s00114-009-0585-y.
Van Leeuwen, T., Been, P., van Herten, M., Zwarts, F., Maassen, B., van der Leij, A., 2007. Cortical categorization failure in 2-month-old infants at risk for dyslexia. NeuroReport 18 (9), 857–861. https://doi.org/10.1097/WNR.0b013e3280c1e2bf.
Vanhatalo, S., Fransson, P., 2016. Advanced EEG and MRI measurements to study the functional development of the newborn brain. In: Neuromethods, Vol. 109. Humana Press Inc.,, pp. 53–68. https://doi.org/10.1007/978-1-4939-3014-2_4.
Vanrumste, B., Van Hoey, G., Van de Walle, R., Michel, R.D., Lemahieu, I.A., Boon, P.A., 2002. Comparison of performance of spherical and realistic head models in dipole localization from noisy EEG. Med. Eng. Phys. 24 (6), 403–418.
Vatta, F., Meneghini, F., Esposito, F., Mininel, S., Di Salle, F., 2009. Solving the forward problem in EEG source analysis by spherical and fdm head modeling: a comparative analysis - biomed 2009. Biomed. Sci. Instrum. 45, 382–388 (Retrieved from). ⟨http://www.ncbi.nlm.nih.gov/pubmed/19369793⟩.
Vorwerk, J., Clerc, M., Burger, M., Wolters, C.H., 2012. Comparison of boundary element and finite element approaches to the EEG forward problem. SUPPL. 1 TRACK-O Biomed. Tech. 57, 795–798. https://doi.org/10.1515/bmt-2012-4152.
Vorwerk, J., Engwer, C., Pursiainen, S., Wolters, C.H., 2017. A Mixed Finite Element Method to Solve the EEG Forward Problem. IEEE Trans. Med. Imaging 36 (4), 930–941. https://doi.org/10.1109/TMI.2016.2624634.
Vorwerk, J., Cho, J.H., Rampp, S., Hamer, H., Knösche, T.R., Wolters, C.H., 2014. A guideline for head volume conductor modeling in EEG and MEG. NeuroImage 100, 590–607. https://doi.org/10.1016/j.neuroimage.2014.06.040.
Vorwerk, J., Oostenveld, R., Piastra, M.C., Magyari, L., Wolters, C.H., 2018. The FieldTrip-SimBio pipeline for EEG forward solutions. Biomed. Eng. Online 17 (1), 1–17. https://doi.org/10.1186/s12938-018-0463-y.
Wang, Y., Gotman, J., 2001. The influence of electrode location errors on EEG dipole source localization with a realistic head model. Clin. Neurophysiol. 112 (9), 1777–1780. https://doi.org/10.1016/S1388-2457(01)00594-6.
Wolters, C.H., Köstler, H., Möller, C., Härdtlein, J., Anwander, A., 2007. Numerical approaches for dipole modeling in finite element method based source analysis. Int. Congr. Ser. 1300, 189–192. https://doi.org/10.1016/j.ics.2007.02.014.
Xie, W., Mallin, B.M., Richards, J.E., 2018. Development of infant sustained attention and its relation to EEG oscillations: an EEG and cortical source analysis study. Dev. Sci. 21 (3), e12562 https://doi.org/10.1111/desc.12562.
Xie, W., McCormick, S.A., Westerlund, A., Bowman, L.C., Nelson, C.A., 2019. Neural Correlates of Facial Emotion Processing in Infancy. Dev. Sci. https://doi.org/10.1111/desc.12758.